Available online at www.sciencedirect.com
SCIENCE DIRECT®
Engineering Structures 28 (2006) 745–755
ENGINEERING STRUCTURES
www.elsevier.com/locate/engstruct

Experimental study on the fatigue behaviour of welded tubular K-joints for bridges

Ann Schumacher[a,*], Alain Nussbaumer[b]

[a] *Swiss Federal Laboratories for Materials Testing and Research (EMPA), Structural Engineering Research Laboratory, Ueberlandstrasse 129, 8600 Dübendorf, Switzerland*
[b] *Swiss Federal Institute of Technology of Lausanne (EPFL), ICOM - Steel Structures Laboratory, School of Architecture, Civil and Environmental Engineering, 1015 Lausanne, Switzerland*

Received 18 July 2005; received in revised form 7 October 2005; accepted 7 October 2005
Available online 15 November 2005

Abstract

Fatigue tests were carried out on welded circular hollow section K-joints typical to bridges. The tests specimens were large-scale (approximately 9 m long and 2 m high) trusses loaded in the plane of the truss. Measured member stresses showed that a significant proportion of the load in a truss member may be due to bending, underlining the importance of considering correctly this load case in the design of these structures. Measured hot-spot stresses in the joints were compared with hot-spot stresses calculated using the current design guidelines. It was found that the measured values are considerably lower than the calculated values, calling into question the applicability of the design guidelines to these types of (bridge) structures.

The *S–N* fatigue results from the current study, on the other hand, showed that the fatigue resistance of the joints that were tested is lower than the corresponding *S–N* design curves. This means that when the considerably higher calculated hot-spot stress range is applied to the corresponding design curve, the predicted resistance is similar to the resistance predicted using the lower measured hot-spot stresses in combination with the lower measured *S–N* curve too. This has highlighted the importance of relating hot-spot stresses to the appropriate, corresponding *S–N* curves.

Evidence from the fatigue tests has clearly demonstrated the effect of size on the fatigue strength of welded tubular joints. A comparison of fatigue *S–N* results from smaller and larger welded circular hollow section (CHS) joints has shown the same trend indicated in design specifications: a thicker failed member results in a lower fatigue strength. The size correction factor integrated into the *S–N* design curves of the specifications, however, does not seem to represent this significant effect justly. In light of the size effect results presented in this paper and the major influence of this effect on the design of welded CHS joints in general, it is recommended that a soundly based solution with targeted *S–N* curves and a representative size effect should be sought.

Keywords: Welded tubular K-joint; Bridge; Hot-spot stress; Stress concentration factor; Fatigue behaviour; *S–N* curves; Size effect

1. Introduction

In search of new and innovative bridge designs, engineers and architects are employing structural members in configurations previously considered prohibitively complicated and uneconomical. Tubes or circular hollow sections (CHS) are examples of members that are becoming increasingly popular. New cutting, preparation and fabrication techniques are making their use—in particular with respect to the connection between members—more feasible and competitive.

The fatigue behaviour of welded CHS joints is a well-recognised problem in the design of tubular truss structures that persists in many domains. Significant work has gone into the development of design methodologies and guidelines for the fatigue behaviour of welded tubular joints. The majority of this work has been carried out with an emphasis on tubular structures in the offshore industry [1–3].

In comparison with offshore structures, CHS truss bridges exhibit several differences with respect to the welded tubular

* Corresponding author. Tel.: +41 44 823 4339; fax: +41 44 823 4455.
E-mail address: ann.schumacher@empa.ch (A. Schumacher).

0141-0296/$ - see front matter © 2005 Elsevier Ltd. All rights reserved.
doi:10.1016/j.engstruct.2005.10.003

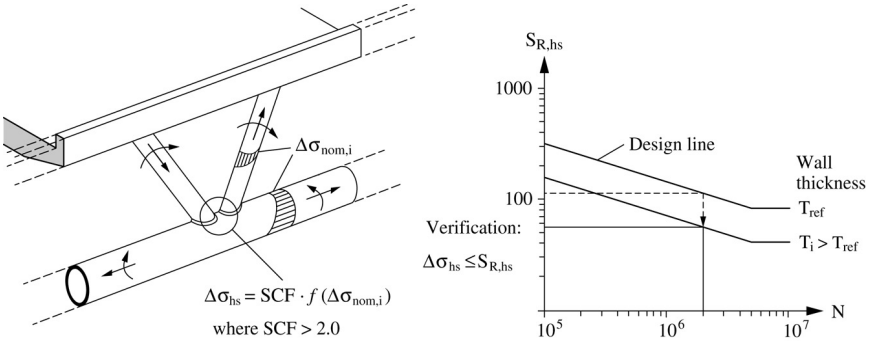

Fig. 1. Fatigue design of welded CHS joints, load effects and resistance.

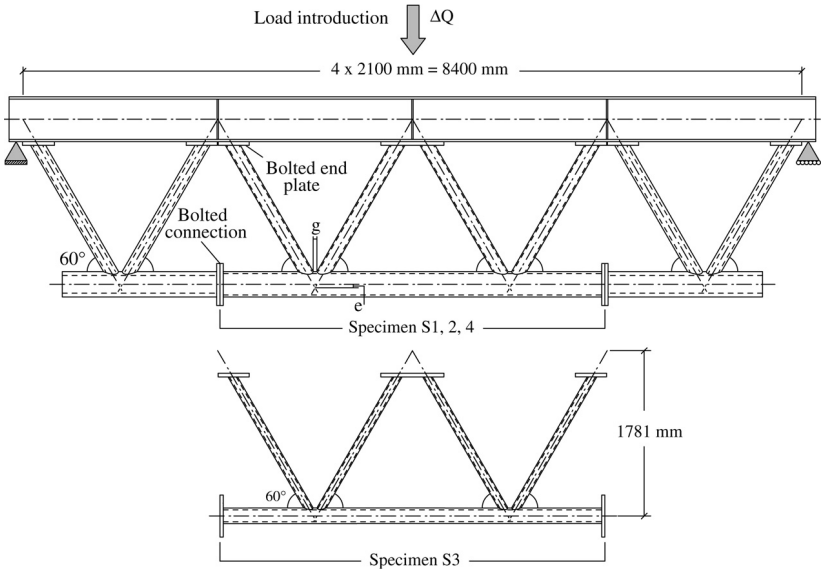

Fig. 2. Truss girder, general configuration and dimensions.

joints: joint geometries, member dimensions (both absolute and relative), the loads affecting the joint, and joint fabrication procedures. When used in the design of CHS truss bridges, current design specifications based on the work done for the offshore industry [4,5] were found to be incomplete and prohibitively conservative. Tubular bridge member dimensions chosen according to static requirements—as is the procedure most commonly used in bridge design—will often fail the subsequent fatigue verification of the joints.

Two main reasons can be identified and are illustrated in Fig. 1. The fatigue design stress, $\Delta\sigma_{hs}$, calculated for CHS bridge joints using empirical parametric equations found in design specifications, is high, typically two to five times higher than the nominal stress, $\Delta\sigma_{nom,i}$, in the truss members. When the design stress is applied to corresponding $S_{R,hs}$–N design lines, a further correction is made depending on the wall thickness, T_i, of the fatigue critical member (chord or brace), which can, in many cases, translate into a further penalty to the fatigue resistance of the joint.

In order to address some of these problems, large-scale tests were carried out to observe and quantify the behaviour of welded CHS K-joints under predominantly fatigue loading [6,7]. Due to the difficulty of performing experimental fatigue investigations on large-scale specimens, the majority of the tests on hollow section joints carried out to date have used isolated joints subjected to simplified loading [8–10]. The tests presented here belong to a relatively small group of tests of this size and configuration. The main aims of the experimental investigation were to measure strains in the truss members in proximity to the brace–chord weld intersection, and to obtain constant amplitude fatigue test results in the form of S–N data and fatigue crack measurements. Comparisons between predicted values calculated using the existing guidelines have also been made.

2. Description of specimens and tests

2.1. Specimens

Eight planar CHS truss girders were tested under static and dynamic load. Fig. 2 shows the general configuration and dimensions of the truss girders. By testing the joints in a truss configuration, it was possible to simulate a realistic load situation. Each truss consisted of four welded CHS K-joints along the bottom chord. Connections between the braces and the top chord, a plate girder, were made using bolted end plates. Due to the location of load application at the centre of the top

Table 1
Test series, nominal values and bridge dimensions

Series (joints)/bridge	Parameter	Nominal dimensions (mm)		θ (°)	β (d/D)	γ (D/2T)	τ (t/T)	Weld
		Chord	Brace					
S1 (1, 2, 3, 4)[a]	Ref.	273 × 20	139.7 × 12.5	60	0.51	6.83	0.63	FP, BR
S2 (1, 2, 3, 4)	Back. ring	273 × 20	139.7 × 12.5	60	0.51	6.83	0.63	FP
S3 (1, 2, 3, 4)	Scale	168.3 × 12.5	88.9 × 8	60	0.53	6.73	0.64	FP, BR
S4 (1, 2, 3, 4)	Weld impr.	273 × 20	139.7 × 12.5	60	0.51	6.83	0.63	FP, BR, WI
Aarw. 1997	–	273 × 20	139.7 × 12.5	45	0.48	4.1–5.6	0.40–0.78	FP
Lully 1997	–	508 × 25–50	267 × 11–25	60	0.53	5.1–10.2	0.44–0.50	FP, BR
Dättwil 2001	–	508 × 50	267 × 11–25	60	0.53	5.10	0.22–0.50	FP, BR

FP: Full penetration weld; BR: Backing ring; WI: Weld improved.
[a] S1, for example, refers to test series 1, which includes four joints: S11, S12, S13 and S14.

chord, the two central K-joints were subjected to the highest loads and were thus the critical fatigue details. This central portion, comprising two CHS K-joints, four braces and one continuous chord, will be referred to as the specimen. Once testing of a particular specimen was complete, it was unbolted, removed and the next specimen was moved into the truss.

A total of four test series with two specimens each—thus four CHS K-joints per series—were carried out. Table 1 lists the test series and gives details for each series: nominal dimensions of the CHS K-joints, non-dimensional joint parameters, weld type (with or without backing ring) and (with or without) weld improvement. For brevity, Table 1 lists nominal member dimensions for each series. In subsequent analysis and calculations, however, the measured dimensions were used. The nominal non-dimensional joint parameters were similar for all four test series. Also shown in Table 1 are the nominal dimensions used in welded CHS K- and KK-joints of three existing welded tubular truss bridges. It can be seen that the non-dimensional parameters of the specimens are similar to the non-dimensional parameters of the bridges.

In order to avoid overlap of the brace members and to facilitate welding in the gap region, a positive eccentricity, e, was accepted between the brace and bottom chord axes (refer to Fig. 2). The eccentricity of a K-joint can be defined as the vertical distance between the chord axis and the intersection point of the two brace axes. In the case of zero eccentricity, the brace axes intersection and the chord axis coincide. For a positive eccentricity the brace axes intersection falls below the chord axis, while for a negative eccentricity the brace axes intersection falls above the chord axis. Although a nominal eccentricity of $e = +38$ mm was specified for all specimens, fabrication tolerances resulted in slightly variable eccentricities between joints.

The material used for the truss members is a hot finished steel of grade S 355 J2 H conforming to EN 10210-1:1994 and EN 10210-2:1997. This refers to a weldable steel with a minimum tensile yield stress, f_y, of 355 N/mm^2 (for nominal thicknesses $\leq$16 mm) or 345 N/mm^2 (for 16 mm $<$ nominal thickness $\leq$40 mm), and a minimum ultimate tensile stress, f_u, between 490–630 N/mm^2 at 22% elongation. The minimum toughness of the steel is defined by 27 J at -20 °C.

Brace members were cut to fit the outer contour of the chord member using computer guided cutting technology. At the same time, bevels were prepared at angles ranging between 30° and 45°. In this way a fully penetrated weld could be applied continuously around the brace–chord intersection. A flux cored arc weld process using covered electrodes in accordance with AWS A5.20:E71 T-1 was used for all specimens.

For series 1, 3 and 4, backing rings (analogous to backing bars for plated joints) were used for the brace–chord weld. The backing rings provide a surface against which the initial weld pass can be made. This method of fabrication was also used for the Lully and Dättwil bridges (see Table 1) and was thought to facilitate the welding procedure and help ensure a fully penetrated weld. In series 4 the test joints were post-weld treated by needle peening following the recommendations in [11]. The aim of the test series was to investigate the positive influence of post-weld treatment on a region of the joint particularly susceptible to fatigue cracking. The treatment was applied to fully fabricated specimens at the chord crown toe region at the base of the tension brace from the gap to the saddle, on both sides of the brace, as shown in Fig. 3.

2.2. Measurements

Strain measurements on truss members were taken during the static tests. Brace and chord members were equipped with uni-axial electrical resistance strain gauges at locations away from the joints. Gauges were positioned in pairs, at either two or four points on a cross-section. Strains in proximity to the brace–chord weld intersection, that is, hot-spot strains, were measured with various types of gauges: uni-axial strain gauges, uni-axial strip gauges, rosettes, and strip rosettes. The gauges were placed at specific joint "hot-spots", that is, locations at the brace–chord intersection where cracks were more likely to initiate under fatigue loading. The typical gauge arrangement used in the tests is shown in Fig. 4.

A second technique was used to measure strains in the joints. The purpose of these measurements was, on one hand, to verify the strains measured with electrical resistance strain gauges and, on the other hand, to obtain a more complete picture of the strain evolution immediately adjacent to the weld toe. To achieve these two objectives, a method based on optical interferometric techniques, specifically speckle interferometry, was adopted. Unlike strain gauges that give measurements at discrete points, speckle interferometry can capture displacements over a quasi-continuous surface [12]. The advantage of this feature for the tests described here was

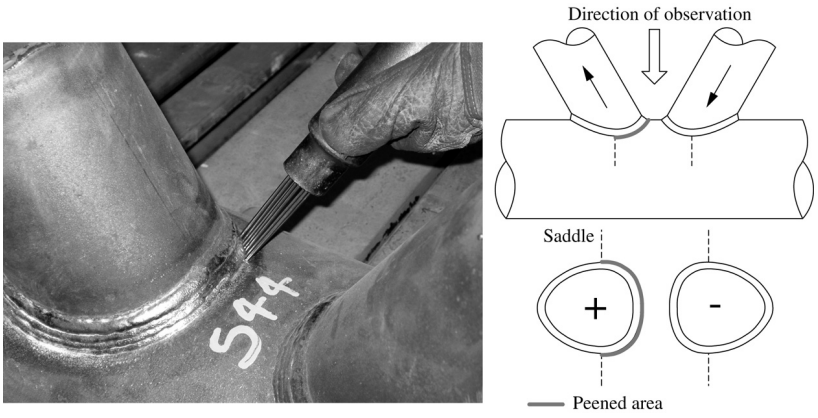

Fig. 3. Needle peening of S44 specimen (left), and treated region of joint (right).

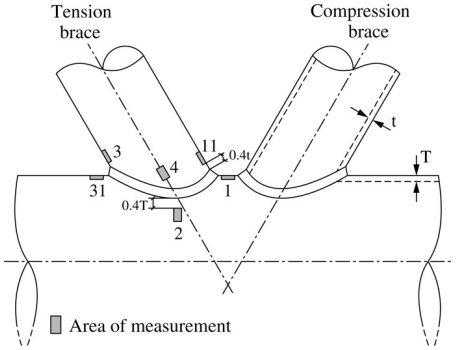

Fig. 4. Typical gauge arrangement on joint; numbered joint locations.

that the strain very close to (or even up to) the weld toe could be measured.

Speckle interferometric techniques rely on the capability of a rough surface illuminated by a laser to retro-diffuse a randomly varying field that appears as a noisy and spotted pattern called speckle. Depending on the optical configuration used, this pattern modifies point by point in relation to the local displacement undergone by the surface. The optical system can convert this local displacement into an optical path difference, which is the visible and measurable output of the system.

Speckle interferometric measurements were not used systematically, for each test, as was the case for the strain gauge measurements. Although optical measurement techniques have been used for decades in civil engineering applications, their in-situ application for large-scale testing still highlights certain practical problems. Thus, strains in only two joints were measured using speckle interferometry: joints S22 and S44. These strains could be compared with concurrently tested and strain gauged joints in the same specimen, i.e. S21 and S43, respectively. Speckle interferometry measurements were only carried out in the gap region of the K-joints (at location 1 in Fig. 4), again due to limitations related to the setup of the optical equipment.

2.3. Test procedure

As shown schematically in Fig. 2, the top chord of the truss girder was simply supported at its extremities. Load (ΔQ) was introduced by a system of two hydraulic jacks acting on a short distribution beam, located at the mid-span of the girder. As a first step, each specimen was subjected to 10 load–unload sequences between the minimum and maximum loads required in the subsequent fatigue test. This was done to ensure that the effect of residual stresses in the truss (either due to the welding and assembly work or small misalignments due to fabrication tolerances) had stabilised and strain range values could be expected to remain constant for the initial stage of fatigue testing. Once stabilised, static strain gauge measurements were taken at the minimum and maximum load levels.

For the fatigue tests, load cycles were applied to the truss in order to determine the number of cycles to crack initiation and to joint failure. Fatigue loading was applied in the form of a sinusoidal wave at a frequency of about 2 Hz, with a load ratio of $R = 0.1$. A load control system was used whereby the load remained constant irrespective of the deflections provoked in the truss girder. Specimens with nominally identical dimensions (series S1, S2 and S4) were subjected to the same minimum and maximum loads. The load applied to the smaller specimens (S3) was adjusted so as to obtain similar nominal stresses in the specimen brace members to those measured in the larger specimens.

The CHS joints were monitored closely during testing to ensure the early detection of fatigue cracking. Once the cracks had been detected, their surface lengths were measured using a dye penetrant technique. The accuracy of this method for measuring the length of surface cracks was verified by measuring crack lengths using magnetic particle inspection. It was found that crack lengths determined with dye penetrant were accurate to within 5 mm. Cracks were measured at regular intervals during fatigue testing.

Joint failure was taken as through-thickness cracking of the chord; since all cracks occurred in the chord, through-cracking could be detected by pressurising slightly the air within the chord and monitoring the pressure with a small mechanical pressure gauge. Once the pressure gauge indicated zero, it was known that one of the two K-joints in the specimen had attained through-cracking. Depending on the surface length of the crack in the second joint, fatigue testing was continued without repair of the failed joint. In all specimens except for S1 (1, 2), cracks were present in the second joint by the time the first joint had

Table 2
Measured member stresses and stress ratios, $\Delta Q = 600$ kN

Joint	Tension brace		Compression brace		Chord	
	$\Delta\sigma_{nom\_br}$ (N/mm^2)	$\sigma_{nom\_br}/\sigma_{ax\_br}$	$\Delta\sigma_{nom\_br}$ (N/mm^2)	$\sigma_{nom\_br}/\sigma_{ax\_br}$	$\Delta\sigma_{nom\_ch}$ (N/mm^2)	$\sigma_{nom\_ch}/\sigma_{ax\_ch}$
S11[a]	78	1.63	−58	1.25	–	–
S21	72	1.66	−53	1.18	6	0.43
S23	74	1.73	−59	1.28	12	0.57
S31	72	1.44	−59	1.16	36	0.95
S33	77	1.38	−61	1.19	40	1.03
S41	81	1.88	−59	1.28	12	0.54
S43	76	1.64	−60	1.35	–	–

[a] S11: series 1, joint 1; S23: series 2 joint 3.

formed a through-thickness crack. For joint S11 the crack was repaired by gouging and re-welding, and testing was continued until cracking in S12 had occurred.

The number of fatigue load cycles was recorded and correlated to events during testing: the detection of a crack (N_2), various stages of crack propagation, and joint failure (N_3) (defined, in this case, as through-thickness cracking of the chord wall). The number of cycles was used to produce $S_{R,hs}$–N data for the test joints.

3. Experimental stress results

3.1. Nominal member stresses

The strains measured in the members are important indicators of the strain arriving at the joint and thus affecting the fatigue behaviour of the joint. Due to joint rigidity, members will not only be subjected to axial strains but also to bending strains that vary over their length. Otherwise stated, the nominal strain (ε_{nom}) measured by the member strain gauges can comprise contributions from several load cases: axial strain (ε_{ax}) due to an axial load, in-plane bending strain (ε_{ipb}) due to in-plane bending, and strain due to out-of-plane bending (ε_{opb}), that is, bending out of the plane of the truss. In the tests described here, the planar nature of the test truss resulted in negligible strains due to out-of-plane bending. As mentioned previously, gauges measuring nominal member strains were placed at certain points along the members. Due to the predominantly uni-axial strain state in the members, the measured strains could be converted into stresses using the simplified Hooke's law.

In the design of tubular trusses, member bending stresses must be accounted for not only in the choice of member dimensions to satisfy static requirements but also in the calculation of fatigue stresses, that is, hot-spot stresses, in the joint. Simulation of the joint rigidity, however, is a difficult task that generally requires three dimensional modelling of the joint. Alternatively, current specifications [4,5] recommend that the truss is modelled with simple bar elements and idealised joints. In this case, additional magnification factors must be used to account for the secondary moments not accurately simulated by the model.

Examining the results presented in Table 2, it can be seen that the proportion of measured bending in the tension braces ($\sigma_{nom\_br}/\sigma_{ax\_br}$) is high. In fact, the nominal-to-axial stress ratios in these members are significantly higher (between 1.5 and 1.8) than the 1.3 magnification factor generally called for in specifications. This high proportion of bending could be due to various factors particular to the truss girders used for the tests, including their stiff joints—a very low γ parameter ($\gamma < 12.0$) was used for the joints, thus making them stiffer than the joints covered in the specifications ($\gamma \geq 12.0$). Furthermore, the test truss was subjected to point loading, which may have produced a more pronounced change in curvature in the two test joints compared to a uniformly distributed load.

The stress ratios in Table 2 also indicate the direction of bending moment with respect to the joint. That is, a ratio of less than unity ($\sigma_{nom}/\sigma_{ax} < 1.0$) means that the bending moment adds compressive strain to the gap region of the joint, as is seen in almost all of the chord members. It is not possible to account for a reduction in axial stress due to compressive bending moments in the simplified modelling procedure described above, that is, magnification factors given in the specifications to account for bending are always greater than one (for CHS K-joint chord members, this factor is 1.5).

Two similar, statically point-loaded large-scale trusses composed of rectangular hollow sections (RHS) with welded K-joints ($\beta = 0.625$, $\gamma = 8.5$, $\tau = 1.0$, $\theta = 60°$) [13], tested to determine the axial force and bending moment distributions in the members, provide a comparison for the present experimental investigation. For the RHS trusses, the stress ratios in the members (comparable to the values presented in Table 2) under serviceability loading, at the location of measurement, were up to 1.02 in the braces (both trusses showed similar values for the brace members), while the stress ratios in the chords varied slightly according to the stiffness of the truss: with a maximum value of 1.06 in the stiffer truss and 1.02 in the less stiff truss (assuming, for simplicity, that the bending moment stress had the same sign as the axial stress at the joint)

Although the stress ratios measured by Frater and Packer [13] were significantly lower than the present measured stress ratios (and significantly lower than the magnification factors generally called for in the specifications), the general trends seen in the two studies are similar. The stiffer RHS truss T_1 (that is, globally stiffer due to larger chord members, other parameters remaining the same) exhibited larger stress ratios in the chords than the less stiff truss, T_2. A similar trend was

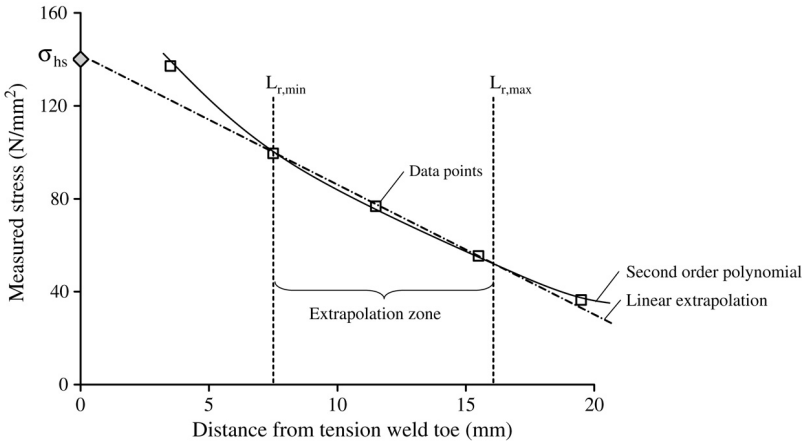

Fig. 5. Extrapolation of data points to determine hot-spot stress at weld toe (stresses from joint S21 shown).

seen in the present investigation, whereby the joints in the stiffer trusses were affected by a larger proportion of bending stress than the joints in the less stiff trusses (compare joints S11, S21 S23, S41, S43 to joints S31 and S33) in both the brace and chord members. This trend appears reasonable, since a globally stiffer truss can be expected to act more like a Vierendeel truss and thus transmit more secondary moment in its members.

3.2. Stresses in joints

The strains measured at joint locations were also converted into stresses. In the multi-axial stress state region of the joint, the relationship between stresses and strains can be described using the generalised Hooke's law, where x is the direction of the axis of interest, in this case perpendicular to the weld toe:

$$\sigma_x = \frac{E}{1-\nu^2}(\varepsilon_x + \nu(\varepsilon_y + \varepsilon_z)) \quad (1)$$

where σ_x is the stress in the direction perpendicular to the weld toe, E is the modulus of elasticity, ν is Poisson's ratio, ε_x is the strain in the direction perpendicular to the weld toe, ε_y is the strain perpendicular to directions x and z, and ε_z is the strain perpendicular to x and y. When it is assumed that the strains ε_y and ε_z are very small ($\varepsilon_x \gg \varepsilon_y, \varepsilon_z$) and taking Poisson's ratio as 0.3, Eq. (1) reduces to:

$$\sigma_x = \frac{E}{1-\nu^2}\varepsilon_x = \frac{E}{0.91}\varepsilon_x = 1.1E\varepsilon_x \quad \text{that is } \frac{\sigma_x}{E\varepsilon_x} = 1.1. \quad (2)$$

Numerous investigations into the validity of Eq. (2) have been made [3,14,15]. They have found that the stress–strain ratio can vary depending on the load level and the location in the joint, but that the average value falls at approximately 1.1 for rectangular hollow section (RHS) joints and 1.2 for CHS joints. Rosette measurements were used to determine the stress–strain ratio in the present study. The measured ratios were found to be similar to the ratios found in the investigations cited above. A value of 1.17 was subsequently used, in accordance with the value found by van Wingerde et al. [16] in their treatment of a large database of joint hot-spots strain results.

As described in Section 2.2, the joints were equipped with various types of gauges, including uni-axial and rosette strip gauges. An example of a strip gauge measurement close to the weld toe at hot-spot location 1 of joint S21 is shown in Fig. 5. Joint hot-spot stresses were determined by extrapolating the stress distributions, such as those shown in Fig. 5, to the weld toe. The hot-spot stress is assumed to include global effects such as joint geometry and the type of load, but excludes local effects due to the weld shape and radius of the weld toe (notch effects) [5].

The extrapolation method to find the hot-spot stress has been studied and discussed thoroughly [3,14,15,17]. For the work presented here, an extrapolation method recommended in [3] was used. For this method a second order polynomial was fitted to the stress data points within defined limits of extrapolation (Fig. 5). A linear extrapolation to the weld toe was then carried out from two points: from the points on the second order polynomial at $L_{r,\min}$ and $L_{r,\max}$. The hot-spot stress, σ_{hs}, was then taken as the value of linearly extrapolated stress at the weld toe.

Fig. 6 shows the distribution of measured stresses at hot-spot location 1, on the chord at the base of the tension brace (refer to Fig. 4) due to a fatigue load $\Delta Q = 600$ kN, for both strain gauge and speckle interferometry measurements. Stresses obtained from the strain gauge measurements are shown at a spacing of 2 mm (series S3) and 4 mm (series S1, S2 and S4). Although gauges were also placed closer than $L_{r,\min}$ for comparison with the speckle results, a minimum of three strain gauges within the extrapolation zone was required in order to make possible extrapolation using a second order polynomial. For the speckle measurements, stresses at intervals of 0.08 mm (quasi-continuous) were obtained, starting directly at the weld toe. In Fig. 6 it can be seen that, due to the geometric perturbation in the joint, the stresses increase relatively rapidly close to the weld toe.

The stresses from the two measuring systems compare fairly well, especially considering that the measurements were taken on different joints, with slightly different nominal member loads, weld shapes and gap sizes. The relatively good concordance between gauge and speckle results was useful, since it served as an independent verification of the strain gauge measurements. The speckle interferometry measurements in Fig. 6 show a smooth, essentially symmetric curve over the

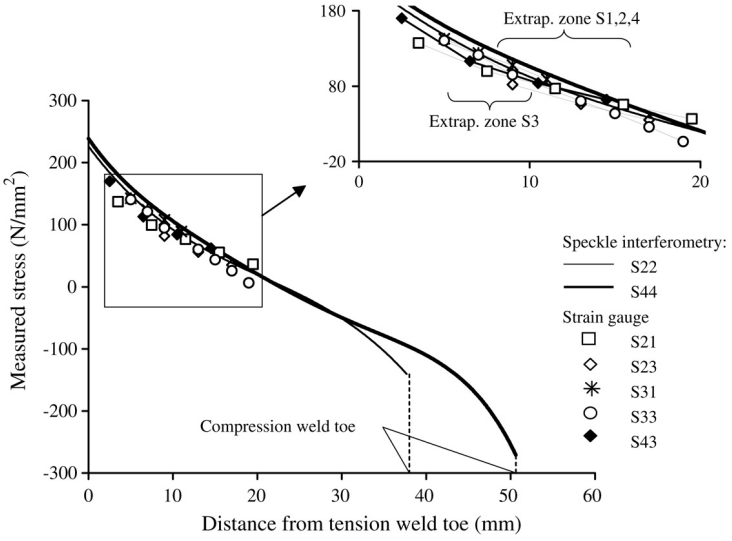

Fig. 6. Stress evolution in K-joint gaps (hot-spot location 1, on chord), from speckle interferometry and strain gauge measurements.

Table 3
Stresses in members and joints, measured and calculated

Location on joint	Joint	Nominal member stresses (N/mm^2)		Hot-spot stresses (N/mm^2)		Ratio
		$\Delta\sigma_{\text{nom\_br}}$	$\Delta\sigma_{\text{nom\_ch}}$	$\Delta\sigma_{\text{hs,meas}}$	$\Delta\sigma_{\text{hs,calc}}$	$\sigma_{\text{hs,calc}}/\sigma_{\text{hs,meas}}$
1	S21	72	15	140	269	1.92
	S31	72	36	187	315	1.68
2	S11	78	11	68	156	2.29
3	S11	78	11	17	167	9.82
4	S11	78	11	67	88	1.31
11	S11	78	11	132	–	–
	S31	72	36	122	–	–

entire gap distance. It can be seen that the inflection point of the curve lies slightly to the left of the point of zero stress. This is due to tension in the chord, which has the effect of increasing the tension in the gap and shifting the curve towards the tension brace.

3.3. Comparison of measured and calculated joint stresses

Hot-spot stresses obtained from the distributions such as those shown in Fig. 6 and at other joint locations are presented in Table 3. They are compared with values calculated using design guidelines and background documents on which the design guidelines are based [18]. For comparison purposes, the nominal stresses in the tension brace and chord member are also given in Table 3. A generalised equation for the calculation of hot-spot stress can be written as follows:

$$\sigma_{\text{hs},i} = \sigma_{\text{ax\_br}} \cdot \text{SCF}_{i,\text{ax\_br}} + \sigma_{\text{ipb\_br}} \cdot \text{SCF}_{i,\text{ipb\_br}} + \sigma_{\text{ax\_ch}} \cdot \text{SCF}_{i,\text{ax\_ch}} + \cdots \quad (3)$$

where, $\sigma_{\text{hs},i}$ is the hot-spot stress at location i, $\sigma_{\text{ax\_br}}$ is the stress in the tension brace due to the axial brace force, $\text{SCF}_{i,\text{ax\_br}}$ is the stress concentration factor at location i due to the axial brace force, $\sigma_{\text{ibp\_br}}$ is the stress in the tension brace due to the in-plane bending moment, $\text{SCF}_{i,\text{ipb\_br}}$ is the stress concentration factor at joint location i due to the moment in the brace, $\sigma_{\text{ax\_ch}}$ is the stress in the chord due to the chord axial force, $\text{SCF}_{i,\text{ax\_ch}}$ is the stress concentration factor at joint location i due to the axial chord force, and so on.

The stress concentration factors (SCFs) for a specific load case can be calculated using parametric equations such as those found in the design guidelines [4,5]. Since the goal of the comparison was to evaluate the validity of the parametric equations in the determination of the hot-spot stress, the measured nominal member stresses from the tests were used in the calculation rather than nominal member stresses determined through analysis of a simple bar element model of the truss (the usual procedure in design). Note that Table 3 makes a comparison of hot-spot stresses and not SCFs. A direct comparison of measured and calculated SCFs for individual load cases could not be made here, since the hot-spot stresses measured in the tests were due to a combination of load cases. Furthermore, in order to calculate the hot-spot stresses, the parametric equations were assumed to be applicable to the test joint geometries. This is not necessarily the case, since the test joints had a lower chord diameter-to-thickness (γ) ratio than covered by the specifications.

In Table 3 it is seen that location 1 is the point of highest measured and calculated hot-spot stresses (series S1 and S2 joints can be compared directly), which corresponds to the fatigue test results—location 1 was the location of cracking for test series S1, S2 and S3. It is also seen that the calculated

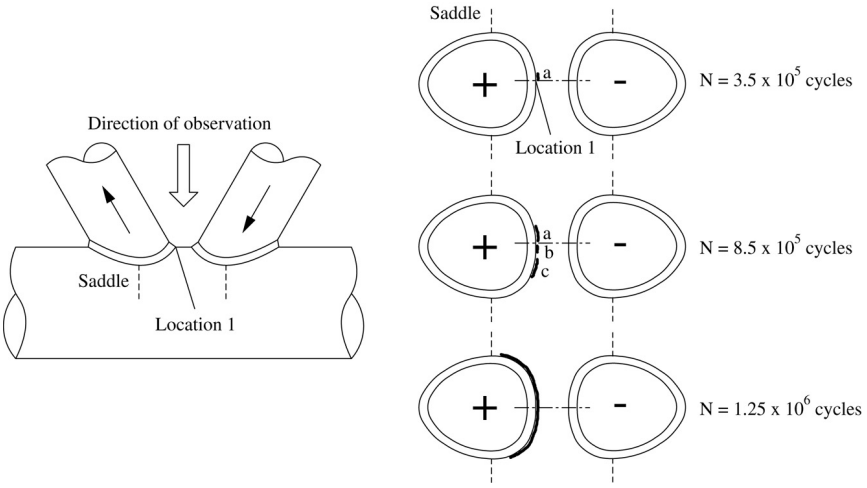

Fig. 7. Fatigue crack development in joint S21.

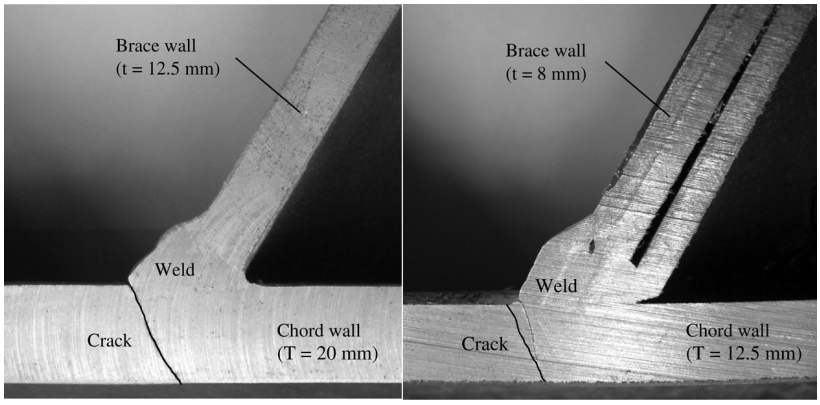

Fig. 8. Cracks through chord thickness: joints S24 (left) and S31 (right) at joint location 1.

hot-spot stresses are systematically higher than the measured stresses. This discrepancy is referred to again below; it was also investigated in detail using a validated finite element model and is reported in [6]. Calculated hot-spot stresses that are too high can be considered conservative. It is possible that these conservative calculated hot-spot values may contribute to an over-design of the structure that will make it economically uncompetitive—this is particularly relevant to bridge structures. It is noted that, for S1 and S2 joints, the measured hot-spot stresses on the brace at location 11 (refer to Fig. 4) were also relatively high. Hot-spot stresses were not calculated for location 11, since parametric equations are not given for this location in the design guidelines. Lastly, the hot-spot stresses measured at location 3 were very low. It is likely that the hot-spot stress at this location, for this particular joint geometry, is not affected by the brace loads. The calculated hot-spot stress at this location, on the other hand, is much higher, since it includes the effect of the brace load.

4. Fatigue behaviour of K-joints

4.1. S–N results

Cracking in all of the series S1, S2 and S3 joints occurred at location 1, that is, at the location of highest measured stress, and followed a similar pattern where cracking occurred approximately symmetrically on either side of location 1 and progressed towards the saddle (location 2), in the chord and along the weld toe, as seen in Fig. 7. Once testing was complete, joints were cut open in order to examine the crack path both in the thickness direction and along the brace–chord intersection. Fig. 8 shows the crack paths through the chord thickness at location 1 for joints S24 and S31. The cracks follow an angled path, that is, they are not perpendicular to the chord surface. This angle is maintained as the cracks propagate along the weld toe, away from location 1, thereby resulting in a so-called double-curved crack. The angled crack indicates that the direction of principal stress (and thus of the crack driving force) at this location is influenced, as expected, by both the brace and chord load. The higher the proportion of brace load (stress), the more the crack angles towards the brace.

The fatigue results for series S1, S2, S3 and S4 are plotted in Fig. 9. The results for S1 and S2 were considered as one data set (S1&2) in light of the similar results obtained for the two series: it was shown that the backing ring (refer to Table 1) did not have an influence on the fatigue behaviour of the joints [6]. The fatigue test results are presented in the form of logarithmically plotted $S_{R,hs}$–N curves, where $S_{R,hs}$ is the hot-spot stress range and N is the number of load cycles to failure. The hot-spot

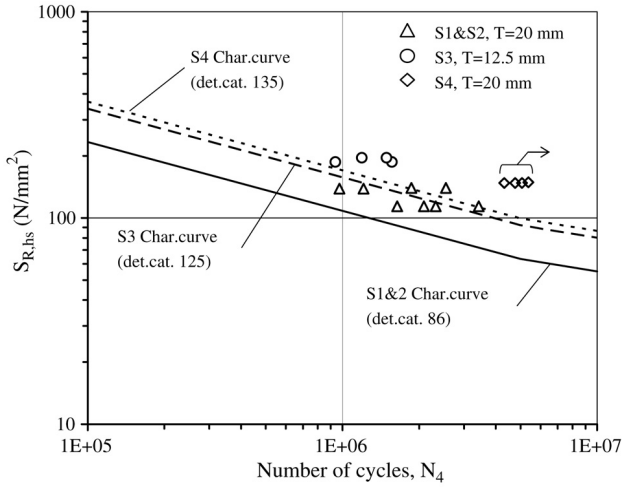

Fig. 9. Fatigue test results for series S1&2, S3 and S4.

stress range is taken at the location of failure: location 1 for all joints. It is noted that the N used in the following figures refers to N_4, that is, the number of cycles at which the joint has suffered a complete loss of strength. Since only N_3 (the number of cycles to through-thickness cracking) was attained in the present tests, a ratio of $N_4/N_3 = 1.49$ found in a study of a large database of fatigue test results of CHS joints [16] was used to extrapolate from N_3 to N_4.

In the statistical evaluation of the test results, $S_{R,hs}$–N mean curves were fitted to the data through regression analysis based on a fixed slope of $m = 3.0$ up to the constant amplitude fatigue limit, $N = 5 \times 10^6$ cycles. At N greater than $N = 5 \times 10^6$ cycles, a slope of $m = 5.0$ was taken. Fixed slopes were used, since all of the specimens were tested at similar hot-spot stress ranges and therefore the experimental determination of a slope was not feasible. Following the determination of a mean curve, characteristic curves (see Fig. 9) were established at a certain number of standard deviations (s_N) of the dependent variable $\log N$ below the mean. By taking an appropriate number of standard deviations below the mean—a value which reflects the number of points in the data set, e.g. $3.5s_N$ for 5 data points, $2.7s_N$ for 10 data points, $2.0s_N$ for 50 data points, and so on [19]—a 95% survival probability with a two-sided 75% confidence level of the mean is achieved. The characteristic curves in Fig. 9 are identified by their $S_{R,hs}$ value at $N = 2 \times 10^6$ cycles (referred to as the detail category).

In Fig. 9 two effects are clearly seen: the effect of size and the effect of post-weld treatment. The effect of size is evident in comparing series S1&2 and S3. The dimensions of the joints in S3 were reduced proportionally in relation to joints in series S1 and S2, while the non-dimensional parameters ($\theta, \beta, \gamma, \tau$) remained roughly the same (refer to Table 1). The data points and their corresponding characteristic curves show that, when the size of the specimen is reduced, the fatigue resistance increases. More specifically, when the thickness of the failed element (in this case the chord, $T_{S1\&2} = 20$ mm, $T_{S3} = 12.5$ mm) is reduced, the characteristic curve is shifted to the right (detail category 86 for S1&2; detail category 125 for S3).

In Fig. 9 the results from series S1&2 can also be compared with the results from series S4. It is recalled that series S4 joints were geometrically identical to S1&2 joints, but were needle peened at and around joint location 1. Testing of the S4 joints was stopped at approximately 3×10^6 cycles (Fig. 9 shows the number of cycles multiplied conservatively by 1.49). At this point, none of the joints in the series had failed, however small fatigue cracks had been detected at location 1 adjacent to the compression brace, referred to as location 1c. The notch at location 1c is nominally the same as at location 1. Although the force in the brace is compressive, the chord at that location is in tension and, more importantly, the material adjacent to the weld is also in tension due to tensile residual weld stresses. Thus, even if the applied stress range is compressive, as was seen in the speckle interferometry results (Fig. 6), the local stress range relevant to fatigue crack growth may be partly or entirely tensile.

Compared with the cracks in the series S1 and S2 joints, the cracks in series S4 joints at location 1c were detected later and propagated at a slower rate, suggesting that the effective stress range was only partly tensile. It is interesting to note that, at a smaller tensile stress range, location 1c is still more critical than other locations around the tension brace–chord intersection, including location 11 on the brace where relatively high hot-spot stresses were measured (Table 3). This raises questions about the comparative severity of the notch at different locations around the joint and whether it is justifiable to compare them on the same basis, for example using the same $S_{R,hs}$–N design curve for hot-spot locations on the chord and on the brace.

Since the tests were stopped prior to through-thickness cracking, a standard deviation for the S4 data points could not be determined. When the standard deviation found for the S1&2 data was applied to the S4 data, however, a comparison in Fig. 9 between the characteristic curves of the two data sets could be made. The increase in the fatigue detail category from detail category 86 to detail category 135—a more than 50% increase in fatigue strength and a three-fold increase in fatigue life—is a very positive result in terms of the potential of needle peening as a method for improving the fatigue behaviour of welded tubular joints. This result is in line with results of other studies where weld improvement techniques have been found to lengthen the fatigue life of welded steel and aluminium plate details [11,20,21].

4.2. Comparison with fatigue design curves

In Fig. 10 the characteristic curves for series S1&2 and S3 are shown, as well as the corresponding $S_{R,hs}$–N design curves. The design curves are based on the reference curve that is valid for joints with failed member thicknesses of 16 mm. This curve can be written as:

$$\log(S_{R,hs,16}) = \frac{1}{3}(12.476 - \log(N_4)) \quad \text{for } 10^3 < N_4 < 5 \times 10^6$$
$$\log(S_{R,hs,16}) = \frac{1}{3}(16.327 - \log(N_4)) \tag{4}$$

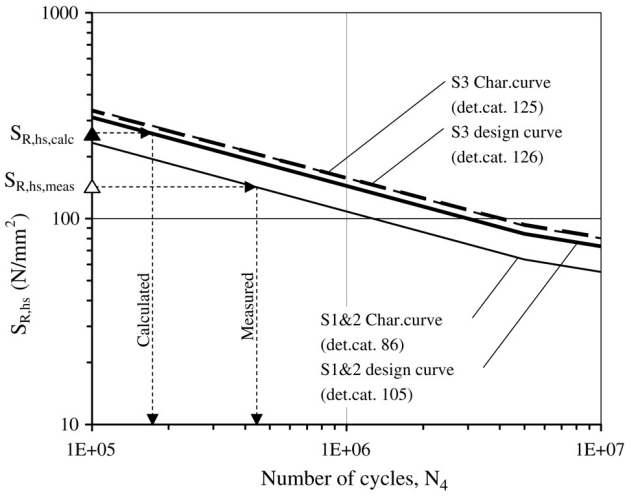

Fig. 10. Comparison of characteristic curves to design curves.

$$\text{for } 5 \times 10^6 < N_4 < 10^8. \tag{5}$$

For thicknesses other than 16 mm, the following corrections are applied to Eqs. (4) and (5), respectively:

$$\frac{S_{R,hs,T}}{S_{R,hs,16}} = \left(\frac{16}{T}\right)^n \quad n = 0.06 \cdot \log N_4 \quad \text{for } 10^3 < N_4 < 5 \times 10^6 \tag{6}$$

$$\frac{S_{R,hs,T}}{S_{R,hs,16}} = \left(\frac{16}{T}\right)^n \quad n = 0.402 \quad \text{for } 5 \times 10^6 < N_4 < 10^8 \tag{7}$$

where $S_{R,hs,T}$ is the hot-spot stress range for tube wall thickness T, $S_{R,hs,16}$ is the hot-spot stress range for a reference tube wall thickness $T_{ref} = 16$ mm, T is the thickness of the failed member, n is the size effect exponent, and N_4 is the number of cycles to failure.

The measured and calculated hot-spot stress ranges at the location of cracking for joint S21 are shown in Fig. 10. The calculated hot-spot stress value was presented previously in Table 3 (joint S21, location 1). When the considerably higher calculated hot-spot stress range is applied to the corresponding design curve (design curve for $T = 20$ mm), it seems that the predicted resistance (in terms of cycles) is too conservative. However, when the measured hot-spot stress range is subsequently related to the $S_{R,hs}$–N curve found from the tests (characteristic curve S1&2), the difference between the predicted and measured number of cycles to failure is no longer great, especially when the N_4 values in the measured case in Fig. 10 are based on a nominal ratio of $N_4/N_3 = 1.49$. This is due to the substantially lower detail category found for series S1&2 in the tests and highlights the importance of relating hot-spot stresses to the appropriate, corresponding $S_{R,hs}$–N curves.

Also seen in Fig. 10 is that the characteristic curve for the S3 results falls at the same level as the design curve for $T = 12.5$ mm, while the characteristic curve for the S1&2 results falls below the design curve for $T = 20$ mm. Based on these results, it appears that the correction for size inherent to the design lines (Eqs. (3)–(6)) may be non-conservative for $T > 16$ mm. Stated otherwise, the observed size effect for proportionally scaled joints appears to be greater than the size correction included in the design lines. It should be recalled, however, that this kind of direct comparison between measured values or curves and those found in the design guidelines is not justifiable (see discussion in previous paragraph). Nevertheless, just concentrating on the measured results, the significant difference in strength between the series S1&2 and S3 has prompted a further investigation into the effect of size. This study, reported in [6] and [22], has highlighted, among other things, the feasibility of simulating the geometric size effect in welded tubular joints through the use of simple linear elastic fracture mechanics models. It also found that the size effect exponent given in Eqs. (5) and (6) was derived from test data of predominantly thinner joints ($T \leq 16$ mm), thus making it questionable whether it is suitable for the thicker bridge joints (i.e. $T > 16$ mm).

The size effect correction has, as it is represented in the design guidelines today, a major influence on the fatigue design of welded tubular joints. When comparing the fatigue strength (stress range) of a welded CHS joint with 16 mm thickness at the expected crack location and, for example, the same joint proportionally scaled such that the critical member is now 50 mm thick, a reduction in the predicted fatigue strength of 35% at two million cycles can be expected according to Eqs. (3)–(6). This is particularly noteworthy for welded CHS bridge joints, since chord members in these structures will, in most cases, have wall thicknesses substantially greater than 16 mm. In the past, substantial effort has been put into the precise determination of hot-spot stresses in welded tubular joints. In comparison, however, much less work has concentrated on defining the corresponding $S_{R,hs}$–N curves and the related size effect correction. In light of the results presented here and the major influence of this effect in general, it seems justifiable to seek a soundly based solution with targeted $S_{R,hs}$–N curves and a representative size effect.

5. Conclusions

An experimental investigation on the fatigue behaviour of welded CHS K-joints for bridges has been carried out. The following conclusions can be drawn:

1. The proportion of bending in all of the tension braces of the test girder was seen to be high. The nominal-to-axial strain ratio in these members is significantly higher than the 1.3 magnification factor given in design guidelines.
2. The hot-spot stress ranges calculated for the test joints, based on current design specifications (using the nominal member stresses measured in the tests), were considerably higher than the measured hot-spot stress ranges.
3. $S_{R,hs}$–N results from a data set of eight joints, where failure occurred in the 20 mm thick chord member, have indicated a characteristic curve that is considerably lower than the corresponding $S_{R,hs}$–N curve: detail category 86 versus detail category 105.

4. The fatigue test results from series S4 demonstrate the beneficial influence of needle peening on the fatigue life of the joints. No cracks formed at joint location 1 or at any other locations around the tension brace–chord intersection, even after three times the number of load cycles compared with other similar test series. Small cracks, however, were detected at location 1c, on the chord adjacent to the compression brace weld toe. The shift of the critical location in the joint, both in space and time, is an outcome that will require further study in order to appropriately quantify the potential benefit of weld improvement as applied to welded CHS joints.
5. When the considerably higher calculated hot-spot stress range (see conclusion 2) is applied to the corresponding design curve, it seems that the predicted resistance (in terms of cycles) is too conservative. However, when the measured hot-spot stress range is subsequently related to the $S_{R,hs}$–N curve also found from tests, the difference between the predicted and measured number of cycles to failure is no longer as great. This is due to the substantially lower detail category found for the test joints and highlights the importance of relating hot-spot stresses to the appropriate, corresponding $S_{R,hs}$–N curves.
6. Investigation of the size effect through comparison of fatigue $S_{R,hs}$–N results from smaller and larger welded CHS joints shows the same trend indicated in design specifications: a thicker failed member results in a lower fatigue strength. The characteristic curve for the smaller joints falls at the same level as the current design curve for $T = 12.5$ mm, while the characteristic curve for the larger joints falls below the current design curve for $T = 20$ mm (see previous conclusion). Based on these results, the correction for size inherent to the design curves appears non-conservative for $T > 16$ mm. In light of the results presented in this paper concerning the size effect and the major influence of this effect on the design of welded CHS joints in general, it seems justifiable to seek a soundly based solution with targeted $S_{R,hs}$–N curves and a representative size effect.

Acknowledgements

The work described herein was sponsored by the Office of the Swiss Federal Highway Administration (ASTRA). Material for the test specimens was contributed by Vallourec & Mannesmann Tubes, Germany.

References

[1] Wordsworth AC, Smedley GP. Stress concentrations at unstiffened tubular joints. In: European offshore steels research seminar. Proceedings, Paper 31. 1978.
[2] Efthymiou M, Durkin S. Stress concentrations in T/Y and gap/overlap K-joints. In: Behavior of offshore structures. The Netherlands: Delft; 1985. p. 429–40.
[3] Romeijn A. Stress and strain concentration factors of welded multiplanar tubular joints. Ph.D. thesis. The Netherlands: Delft University of Technology, Delft University Press; 1994.
[4] Zhao XL, Packer JA, editors. IIW (International Institute of Welding). Fatigue design procedure for welded hollow section joints. Doc. XIII-1804-99, XV-1035-99; 2000.
[5] Zhao XL, Herion S, Packer JA, Puthli RS, Sedlacek G, Wardenier J et al. Design guide for circular and rectangular hollow section welded joints under fatigue loading. In: CIDECT, Comité International Pour le Développement et L'étude de la Construction Tubulaire. Serial No. 8, Köln (Germany): TUV-Verlag Rheinland; 2000.
[6] Schumacher A. Fatigue behaviour of welded circular hollow section joints in bridges. Ph.D. thesis 2727. Switzerland: Ecole Polytechnique Féderale de Lausanne; 2003.
[7] Schumacher A, Sturm S, Walbridge S, Nussbaumer A, Hirt M, Vollmar T. Fatigue design of bridges with welded circular hollow sections. Swiss association of road and transportation experts, Zurich; 2004 (ASTRA Forschungsantrag AGB 1998/103 (88/89)).
[8] Shao Y, Lie ST. Parametric equation of stress intensity factor for tubular K-joint under balanced axial loads. International Journal of Fatigue 2005; 27:666–79.
[9] Sakai Y, Hosaka T, Isoe A, Ichikawa A, Mitsuki K. Experiments on concrete filled and reinforced tubular K-joints of truss girder. Journal of Constructional Steel Research 2004;60:683–99.
[10] Mashiri FR, Zhao XL, Grundy P. Stress concentration factors and fatigue behaviour of welded thin-walled CHS–SHS T-joints under in-plane bending. Engineering Structures 2004;26:1861–75.
[11] Haagensen PJ, Maddox SJ. IIW recommendations on post weld improvement of steel and aluminium structures. IIW Commission XIII, XIII-1815-00; 2001.
[12] Facchini M, Jacquot P. Speckle interferometry measurements in testing halls for civil engineering applications. In: Proceedings of SPIE, Interferometry '99. 1999.
[13] Frater GS, Packer JA. Modelling of hollow structural section trusses. Canadian Journal of Civil Engineering 1992;19(6):947–59.
[14] van Wingerde AM. The fatigue behavior of T- and X-joints made of square hollow sections. Heron 1992;37(2).
[15] Panjeh ShahiE. Stress and strain concentration factors of welded multiplanar joints between square hollow sections. Ph.D. thesis. The Netherlands: Delft University of Technology, Delft University Press; 1994.
[16] van Wingerde AM, van Delft DRV, Wardenier J, Packer JA. Scale effects on the fatigue behaviour of tubular structures. WRC Proceedings IIW. 1997.
[17] Herion S. Räumliche K-Knoten aus Rechteck-Hohlprofilen. Ph.D. thesis. Germany: University of Karlsruhe; 1994.
[18] Karamanos SA, Romeijn A, Wardenier J. Stress concentrations and joint flexibility effects in multi-planar welded tubular connections for fatigue design. Stevin report 6-98-05, CIDECT report 7R-17/98. The Netherlands: Delft University of Technology; 1997.
[19] Hobbacher A. IIW (International Institute of Welding). Fatigue design of welded joints and components. XIII-1539-96/XV-845-96; 1996.
[20] Bremen U. Amélioration du comportement à la fatigue d'assemblages soudès: étude et modelisation de l'effet de contraintes résiduelles. Ph.D. thesis 787. Switzerland: Ecole Polytechnique Féderale de Lausanne; 1989.
[21] Dubois V. Fatigue de détails soudés traités sous sollicitations d'amplitude variable. Ph.D. thesis 1260. Switzerland: Ecole Polytechnique Féderale de Lausanne; 1994.
[22] Schumacher A, Nussbaumer A, Hirt MA. Fatigue behaviour of welded CHS bridge joints: emphasis on the effect of size. In: Proceedings of the 10th international symposium on tubular structures "Tubular Structures X". Madrid: A.A. Balkema Publishers; 2003. p. 365–74.